Journal of Sol-Gel Science and Technology (2022) 103:853–864
https://doi.org/10.1007/s10971-022-05902-0

ORIGINAL PAPER: SOL-GEL AND HYBRID MATERIALS FOR ENERGY, ENVIRONMENT AND BUILDING APPLICATIONS

Mo-modified TiO_2 mesoporous microspheres prepared by spray pyrolysis for adsorption-photocatalytic water remediation

The Ky Vo[1]

Received: 18 April 2022 / Accepted: 3 July 2022 / Published online: 15 July 2022

Abstract

In this work, Mo-modified TiO_2 microspheres (Mo@TiO_2) were rapidly prepared by the spray pyrolysis method. The titania sol solution containing molybdenum salt and citric acid (CA) was nebulized to generate fine droplets, which were continuously transported into a quartz reactor heated at 600 °C by an N_2 gas flow. Characterization results revealed that the prepared Mo@TiO_2 exhibited enhanced porosity and light adsorption ability. In addition, incorporating Mo species into the anatase TiO_2 lattice narrowed the bandgap energy and created oxygen deficiencies, which are beneficial for the photo-reduction performance. The adsorption-photodegradation of tetracycline antibiotics (TE) was systematically optimized by monitoring the Mo loads, catalyst dosage, contaminant concentration, and pH media. The results indicated that the optimal Mo@TiO_2 microspheres containing 3 wt% Mo showed the highest removal efficiency of *ca.* ~90% toward tetracycline antibiotics under UV-light irradiation, surpassing the undoped TiO_2 and commercial TiO_2 (P25). Finally, after several photooxidation cycles, the fabricated Mo@TiO_2 microspheres retained good photocatalytic activity and stability. The findings suggest that the spray pyrolysis-derived Mo-modified TiO_2 microspheres can be promising photocatalytic materials for treating antibiotics in water.

Graphical abstract

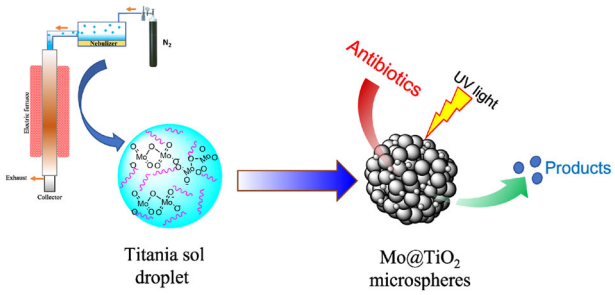

Keywords Sol-gel · Spray pyrolysis · Mo@TiO_2 · Microspheres · Pho-reduction · Tetracycline.

Highlights

- Mesoporous Mo-incorporated TiO_2 microspheres were effectively prepared via sol-spray pyrolysis.
- Mo-modified TiO_2 showed enhanced light absorption ability and porosity.
- Mo@TiO_2 microspheres exhibited improved photo-reduction efficiency under UV-light irradiation.
- Mo@TiO_2 microspheres had good stability and renewability.

✉ The Ky Vo
votheky@iuh.edu.vn

[1] Department of Chemical Engineering, Industrial University of Ho Chi Minh City, 12 Nguyen Van Bao, Go Vap, Ho Chi Minh, Vietnam

1 Introduction

The remediation of organic antibiotics has recently drawn considerable attention owing to their toxicity to aquatic organisms, terrestrial animals, and humans [1, 2]. Furthermore, after releasing in the environment, these organic pollutants can produce multi-resistant bacterial strains that can no longer be handled with the recent drugs [3, 4]. Thus, research on eliminating antibiotics from wastewater has attracted much tension for decays [5–7]. Among known methodologies, photocatalytic oxidation is attracting extensive attention from researchers [3, 8, 9]. Research indicated that the photodegradation efficiency depends on the development of photocatalytic materials. However, there is still a challenge in developing a highly efficient photocatalyst for the photo-reduction of organic pollutants. Recently, metal-organic frameworks (MOFs)-based semiconductors have been applied to photocatalytically degrade organic contaminants [2, 5, 10]. Nonetheless, the production of MOFs is expensive, which hinders them from practical applications [11–13].

The use of metal oxides, such as ZnO [14–16], Cu_2O [17], Fe_3O_4 [18], Fe_2O_3 [19], or TiO_2 [1, 3, 20–23] as photocatalysts for the photo-reduction of organic pollutants has been received much attention for years because they are cost-effective and easily prepared. Among them, anatase TiO_2 is a promising material because it has a high surface area and mesoporous structure, providing active sites for adsorption and photocatalytic performances [1, 20, 21, 23, 24]. Although the bare TiO_2 exhibited a good photo-reduction ability toward organic contaminants, its practical application is still limited because of its poor light absorption and quick recombination of photo-induced species [9, 25–27]. Thus, it needs further to improve the photocatalytic activities and adsorption ability of TiO_2. Research has found that the modification of TiO_2 by Ag [28], Fe_2O_3 [29], graphene oxide [30], g-C_3N_4 [31], chalcogenide [32], or carbon nanotube [33] increased the photocatalytic performance. In addition, Wu et al. [1] discovered that incorporating N into the lattice matrix of TiO_2 significantly increased the photooxidation efficiency of TiO_2. Erdogan et al. [26] reported that dopant elements such as Mo, Fe, and N decreased the bandgap energy of TiO_2, enhancing their photooxidation ability. Recently, Dong et al. [24] found that defective mesoporous TiO_2 showed more photocatalytic activity than defect-free TiO_2. These findings indicated that introducing suitable dopants into the TiO_2 matrix to enhance their photocatalytic activities could be a promising strategy.

Efficient photocatalysts for large-scale water treatment require high catalytic activities, low cost, and facile preparation. So far, TiO_2-based photocatalysts have been mainly prepared using batch mode synthesis, which is challenging to scale up for large-scale production. For instance, Phromma et al. [34] prepared photocatalyst

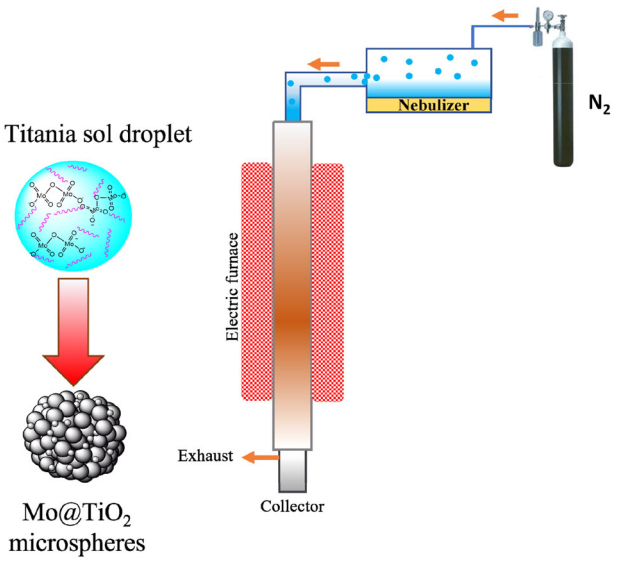

Scheme 1 Schematic diagram of spray pyrolysis of Mo-modified TiO_2 microspheres

TiO_2 nanoparticles via the wet ball milling sol-gel method, which was proceeded with many preparation steps. Thi et al. [23] synthesized Mo-doped TiO_2 using the solvothermal method. Devi et al. [35] prepared M^{n+}-doped TiO_2 (M^{n+}: V^{5+}, Mo^{6+}, and Th^{4+}) by the impregnation method, followed by calcination. Stengl et al. prepared Mo-doped anatase by thermal hydrolysis of Mo and Ti peroxo-complexes from aqueous solutions. However, this method required a very long reaction time, and the produced material had low porosity [36]. Recently, spray pyrolysis synthesis has been widely applied to prepare materials in various fields. The spray pyrolysis-derived materials exhibited enhanced surface area and pore volume than the conventional batch synthesis [37–40]. Notably, spray pyrolysis is easy to scale up for large-scale production because of its continous flow nature.

In this work, Mo-incorporated TiO_2 microspheres were quickly prepared by the surfactant-assisted spray pyrolysis method (Scheme 1). Titania sol containing molybdenum salt and citric acid was ultrasonicated to generate fine droplets, which were continuously transported into a quartz reactor by an N_2 gas flow and pyrolyzed at the desired temperature. Characterization results revealed that the spray pyrolysis-derived Mo@TiO_2 exhibited significantly enhanced surface area and pore volume. In addition, the incorporated Mo species narrowed the bandgap energy of the Mo@TiO_2 samples, enhancing their light absorption ability. Furthermore, the Mo-modified TiO_2 microspheres contained oxygen deficiencies, which improved their photo-reduction efficiency under UV light illumination.

2 Experimental

2.1 Spry pyrolysis synthesis of Mo@TiO_2 microspheres

Mo@TiO_2 microspheres were synthesized by the spray pyrolysis of the titania sol following our work [6, 37]. Briefly, a calculated amount of titanium tetraisopropoxide [Ti $(OC_3H_7)_4$, 97%, Aldrich] was dissolved in isopropanol at room temperature and in a water-free atmosphere. To the resultant solution, deionized water was added slowly under stirring conditions for 3 h. Next, the resultant white precipitates were dispersed in the desired amount of deionized water, then peptized with 1 M HNO_3 to obtain a stable sol. For the spray pyrolysis process, 400 ml titania sol was added with the desired amount of citric acid and ammonium heptamolybdate $[(NH_4)_6Mo_7O_{24}{\cdot}4H_2O$, Aldrich] under stirring conditions. Herein, citric acid acts as a surfactant that enhances the sample's porosity and the metal dopant dispersion. The spry pyrolysis procedure is briefly described in Scheme 1. The obtained product was then calcined at 450 °C for 3 h with a 2 °C/min heating rate in the air to eliminate the carbonaceous material certainly. The final samples are named Mo@TiO_2-x, in which x is the weight percentage of Mo ($x = 1.0$, 3.0, and 5.0 wt%).

2.2 Characterizations

The textural properties of the prepared samples were determined using N_2 porosimetry (ASAP 2020, Micromeritics Instrument Co., USA) at 77 K. Before analysis, the samples were activated at 150 °C under vacuum conditions for 8 h. The specific surface area was determined by a multipoint Brunauer–Emmet–Teller (BET) method using the adsorption data in the relative pressure (P/P0) range of 0.05–0.25. The Barrett–Joyner–Halender (BJH) method with cylindrical pore size estimated from the Kelvin equation was used in the data processing. The crystallographic structures of the samples were analyzed utilizing powder X-ray diffraction (XRD) using an X-ray diffractometer (MAC-18XHF, Rigaku, Japan) equipped with a CuKα radiation source ($\lambda = 1.54$ Å) and operated at a scanning rate of 5°/min from 20° to 80°. The morphologies of the prepared materials were obtained via field-emission scanning electron microscopy (FE-SEM; Leo-Supra 55, Carl Zeiss STM, Germany). The FT-IR absorption analysis was conducted with a Bruker model Tensor 27 in the range of 4000–400 cm^{-1} using KBr powders. An X-ray photoelectron spectrometer (XPS, Thermo Scientific K-Alpha spectrometer) was employed to determine the chemical state of elements. The binding energies were corrected by setting the binding energy of the adventitious carbon (C 1 s) at 284.6 eV. Inductively coupled plasma-optical emission spectrometry (ICP-OES) analyses were carried on with an OPTIMA 8300 (Perkin-Elmer, USA). The photoluminescence (PL) spectra of the samples were analyzed employing an FLS920 fluorescence spectrometer. The optical properties of the samples were analyzed by UV–vis diffuse reflectance spectrophotometer (DRS; UV-2600, Shimadzu, Japan).

2.3 Adsorption and photodegradation experiments

The removal experiments of tetracycline antibiotics ($C_{22}H_{24}N_2O_8$, Aldrich, 99%) was conducted using a photochemical reaction cell assembled with a 300-W Xe-arc lamp. Before use, all samples were degassed at 150 °C under vacuum conditions for 8 h. For each run, 0.15 g of degassed catalyst was added to the TE solution and magnetically stirred for 90 min in the dark. After exposure to UV light irradiation with continuous stirring, the reaction mixture was withdrawn and centrifuged to recover the catalyst; meanwhile, the TE content in the resultant solution was measured employing a UV-visible spectrophotometer (Optizen POP, Mecasys, Korea). The TE removal experiment was also conducted using commercial TiO_2 (P25) for comparison.

3 Results and discussion

3.1 Characterizations

Multi-grams of mesoporous microspheres Mo-doped TiO_2 were quickly obtained by spray pyrolysis. FE-SEM images of the samples produced by the spray pyrolysis method show that all samples exist in uniform spheres with a particle diameter of 0.5–1.5 μm [Fig. 1(a–d)]. EDS dot maps analyses showed that Mo species were finely dispersed throughout the microspheres [Fig. 1(e–h)]. Moreover, the ICP-OES results revealed that the Mo content increased with the Mo/Ti molar ratio, providing direct evidence of controllable loadings of Mo during the spray pyrolysis (Table 1).

The crystallographic structure of the Mo-modified TiO_2 microspheres was examined by XRD analyses, as described in Fig. 2(a). The XRD pattern of the bare TiO_2 exhibited diffraction peaks at $2\theta = 25.6°$, 38.4°, 48.4°, 63.4°, and 76° (JCPDS card No. 21-1272), featuring the anatase-type TiO_2 [37]. As shown, the produced Mo-incorporated TiO_2 samples exhibited the same XRD patterns as the bare TiO_2, suggesting that the incorporation of metal species did not influence the phase structure evolution of the TiO_2 host. Furthermore, there were no characteristic peaks of molybdenum oxides witnessed on XRD patterns of the Mo@TiO_2 samples. This suggests that the incorporated Mo species could be amorphous or well-dispersed within the anatase crystal matrix and

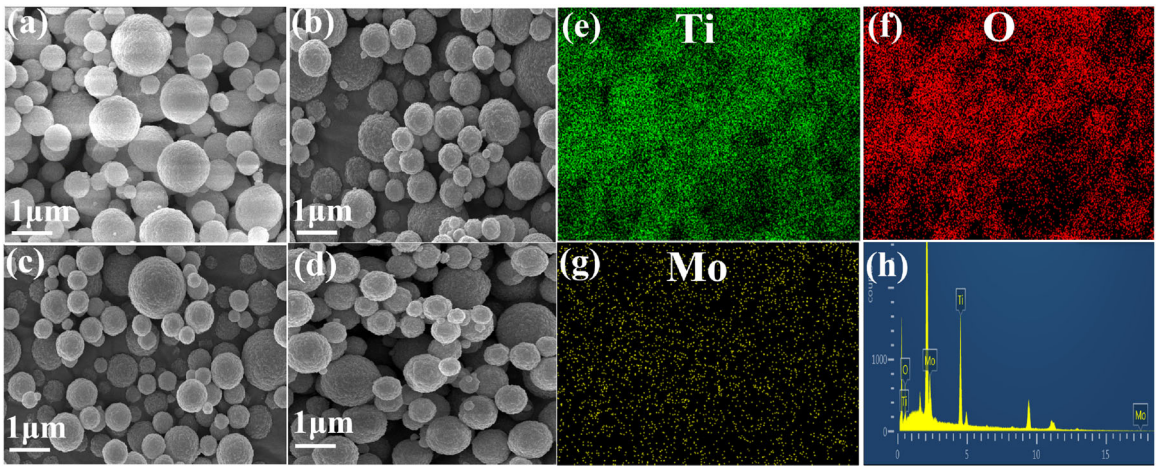

Fig. 1 HR-SEM images of the spray pyrolysis-derived samples. a TiO_2, **b** Mo@TiO_2-1, **c** Mo@TiO_2-3, **d** Mo@TiO_2-5, and **e–h** EDS mapping of Mo@TiO_2-3 sample

Table 1 Textural properties and Mo contents of the synthesized samples

Sample	Mo content*, (wt %)	BET surfaces are, m^2/g	Pore volume, cm^3/g	Mean pore diameter, nm
P25	–	50	–	–
TiO_2	–	119	0.18	5.29
Mo@TiO_2-1	1.10	128	0.21	5.33
Mo@TiO_2-3	2.85	141	0.30	5.41
Mo@TiO_2-5	5.13	152	0.32	5.52

(*) Based on ICP-OES analaysis

beyond the detection limit of XRD [37, 41]. Noticeably, the peaks of TiO_2 slightly shifted right, and the shift magnitude increased with the Mo load [the enlarged Fig. 2(a)]. This implies that Mo species were successfully incorporated into the TiO_2 lattice and caused lattice strains. It should be mentioned that the ionic radius of Mo^{6+} (~0.62 Å) is quite close to that of Ti^{4+} (~0.68 Å). Thus, the Ti^{4+} in the TiO_2 lattice can be substituted by the guest Mo^{6+} ones, which results in a lattice strain within the TiO_2 host [23, 42]. The functional groups of the SP-derived TiO_2 and Mo@TiO_2 microspheres were analyzed via FT-IR spectrum, as demonstrated in Fig. 2(b). The spectrum of the bare TiO_2 microspheres exhibits the vibration modes ~3430 cm^{-1} and ~1640 cm^{-1}, which are ascribable to the adsorbed water molecules. The predominant band at the lower wavenumber of 620 cm^{-1} resulted from the Ti-O-Ti vibration [43]. These bands were slightly moved toward the higher wavenumber on the FT-IR spectra of the Mo-incorporated TiO_2 samples. In addition, the FT-IR spectrum of the Mo@TiO_2-5 sample containing 5 wt% of Mo showed the characteristic vibration peaks of 638, 825, and 915 cm^{-1}, which shifted compared to those of the bulk MoO_3. These shifts could be caused by the newly formed Ti-O-Mo or Mo-Ti-O bonds or the oxygen deficiencies within the TiO_2 crystal [26]. The surface structure of the fabricated TiO_2 and Mo@TiO_2 microspheres was also probed by Raman spectroscopy, as shown in Fig. 2(c). The bare TiO_2 shows the Raman bands at ~138, 388, 508, and 632 cm^{-1}, which were the characteristics of the anatase TiO_2 [21]. These bands shifted and broadened on the spectra of the Mo-modified TiO_2 microspheres. The findings confirmed the distortion and defects of TiO_2 lattice due to the incorporation of Mo species [21]. N_2 sorption and pore size distribution of the TiO_2 and Mo-modified TiO_2 microspheres were analyzed, and the results are shown in Fig. 2(d). The prepared Mo@TiO_2 samples exhibited enhanced N_2 adsorption capacity than the pristine TiO_2. In addition, the pore size of the produced Mo@TiO_2 samples increased with the Mo loads [the inset of Fig. 2(d)]. This is possible because incorporating Mo dopants created new pore structures within Mo@TiO_2. The same phenomenon was previously reported in the literature [37, 44]. From Table 1, the bare TiO_2 microsphere had surface area and pore volume was 119 m^2/g and 0.18 cm^3/g, respectively, which were remarkably higher than the commercial titania. For the Mo@TiO_2 sample, increasing the Mo load from 1.0 wt% to 5.0 wt%, the surface are ranged from 128 m^2/g to 152 m^2/g, respectively; meanwhile, the pore volume ranged from 0.21 cm^3/g to 0.32 cm^3/g, respectively.

The valence states of the elements were analyzed by XPS, and the results are presented in Fig. 3(a–d). The survey scan result of the Mo-doped TiO_2 sample revealed the presence of Mo species [Fig. 3(a)]. The Ti 2p core-level spectrum of the pristine TiO_2 shows a peak at 459. 0 eV and 464.6 eV, ascribed to the Ti $2p_{3/2}$ and Ti $2p_{1/2}$ binding energies, respectively [45] [Fig. 3(b)]. As shown, the incorporation of Mo into the TiO_2 matrix resulted in binding energy shifts of the Ti 2p levels. In addition, the spray-derived Mo@TiO_2 microspheres exhibited broader and

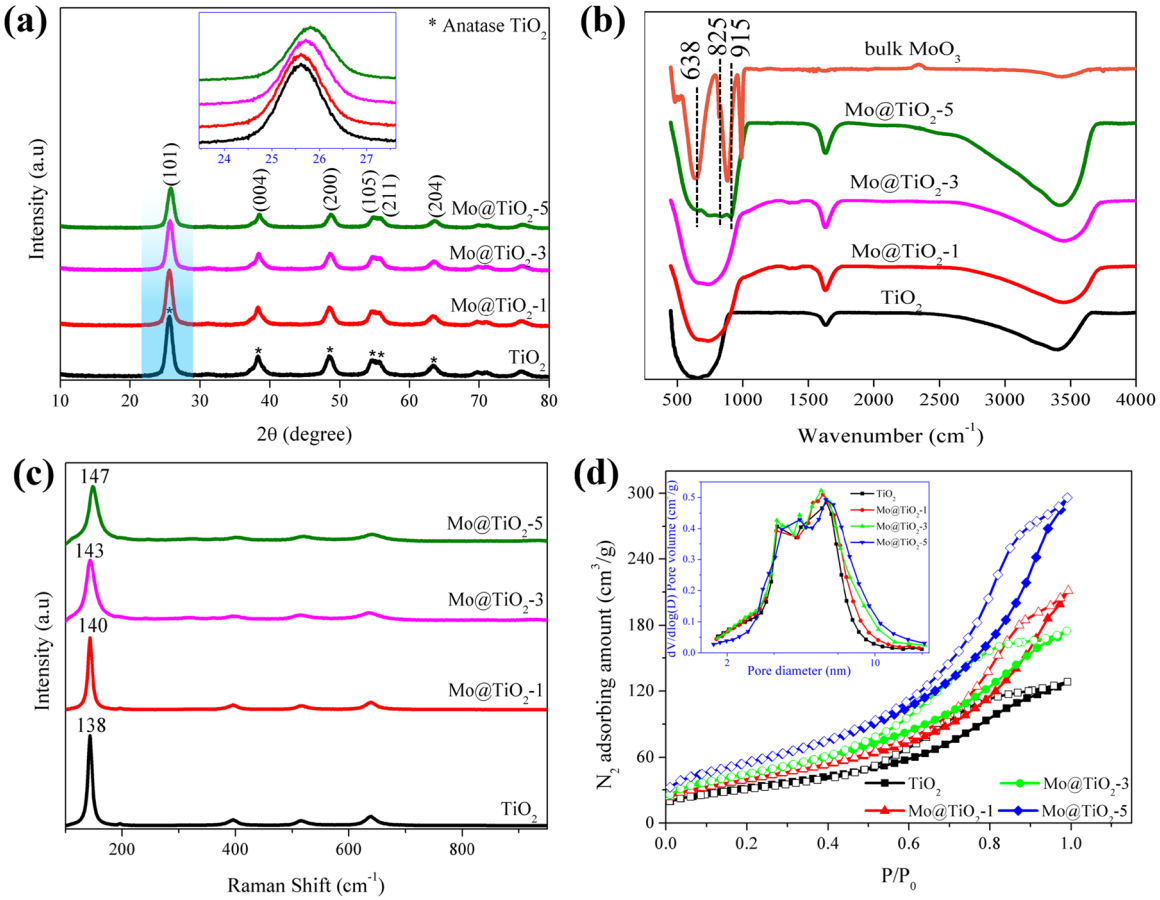

Fig. 2 Characterization of the synthesized samples. a XRD patterns, **b** FT-IR spectra, **c** Raman spectra, and **d** N_2 adsorption–desorption curves

higher binding energy peaks of Ti 2p than the pristine TiO_2 sample. These suggest the crystal structure of TiO_2 anatase could be disordered owing to the Mo guest species. The O 1 s core-level XPS spectrum of the bare TiO_2 exhibited a dominant biding energy peak around 530.3 eV, which is ascribable to the oxygen in the TiO_2 lattice [46]. This peak slightly moved on the spectra of the Mo@TiO_2 catalysts. Besides the oxygen in the titania lattice, the O 1 s spectrum also revealed the presence of adsorbed oxygen (~ 532.1 eV) and adsorbed water and hydroxyl groups (~533.4 eV) [45–47] [Fig. 3(c)]. It is worth mentioning that the concentration of adsorbed oxygen on the Mo-doped TiO_2 catalyst was greatly higher than that on the undoped TiO_2. The findings implied that the Mo@TiO_2 samples contained the surface deficiencies of oxygen, which enhanced their adsorption of oxygen [24, 47, 48]. The Mo 3d core spectra revealed that Mo^{6+} and Mo^{5+} co-existed within the Mo-incorporated TiO_2 microspheres [Fig. 3(d)]. Specifically, the Mo^{6+} state was characterized by the energy peak at ~232.6 eV (Mo $3d_{5/2}$) and ~235.7 eV (Mo $3d_{3/2}$) [37, 49]; meanwhile, the existence of Mo^{5+} species has been proven by the energy peak at ~231.3 eV (Mo $3d_{5/2}$) and ~234.6 eV (Mo $3d_{3/2}$) [37, 49]. As shown in Fig. 3(d), Mo^{6+} was partially reduced to Mo^{5+}, which is undoubtedly evident in the oxygen-deficient states within the TiO_2 lattice [26, 47]. These defects are beneficial for adsorbing oxygen onto the catalyst surface, enhancing the photo-reduction efficiency.

The optical properties of the synthesized TiO_2 and Mo@TiO_2 were investigated via UV-vis diffuse reflection spectroscopy. As demonstrated in Fig. 4(a), the bare TiO_2 predominantly absorbed light in the ultraviolet region. However, the absorption edges of the Mo-incorporated TiO_2 microspheres obviously shifted towards the visible-light region. This suggests that the introduced Mo species could form MoO_{3-x} oxides that are effectively responsive to visible light [50, 51]. Furthermore, the obtained result is consistent with the presence of Mo^{5+} species in the XPS analyses. That is to say, the modification of the TiO_2 anatase by Mo dopants extended the catalysts' absorption edge to the visible light region. The bandgap energy values of the prepared samples were estimated using Tauc's plots, as presented in Fig. 4(b). The pristine TiO_2 anatase had a bandgap energy value of ~3.18 eV, which is consistent with the previous report [47]. However, introducing 1.0 to 5.0 wt% of Mo decreased the bandgap value of anatase TiO_2 from ~3.08 to ~2.93 eV, respectively Fig. 4(b). Research has found that incorporating Mo^{6+} ions within the TiO_2 lattice

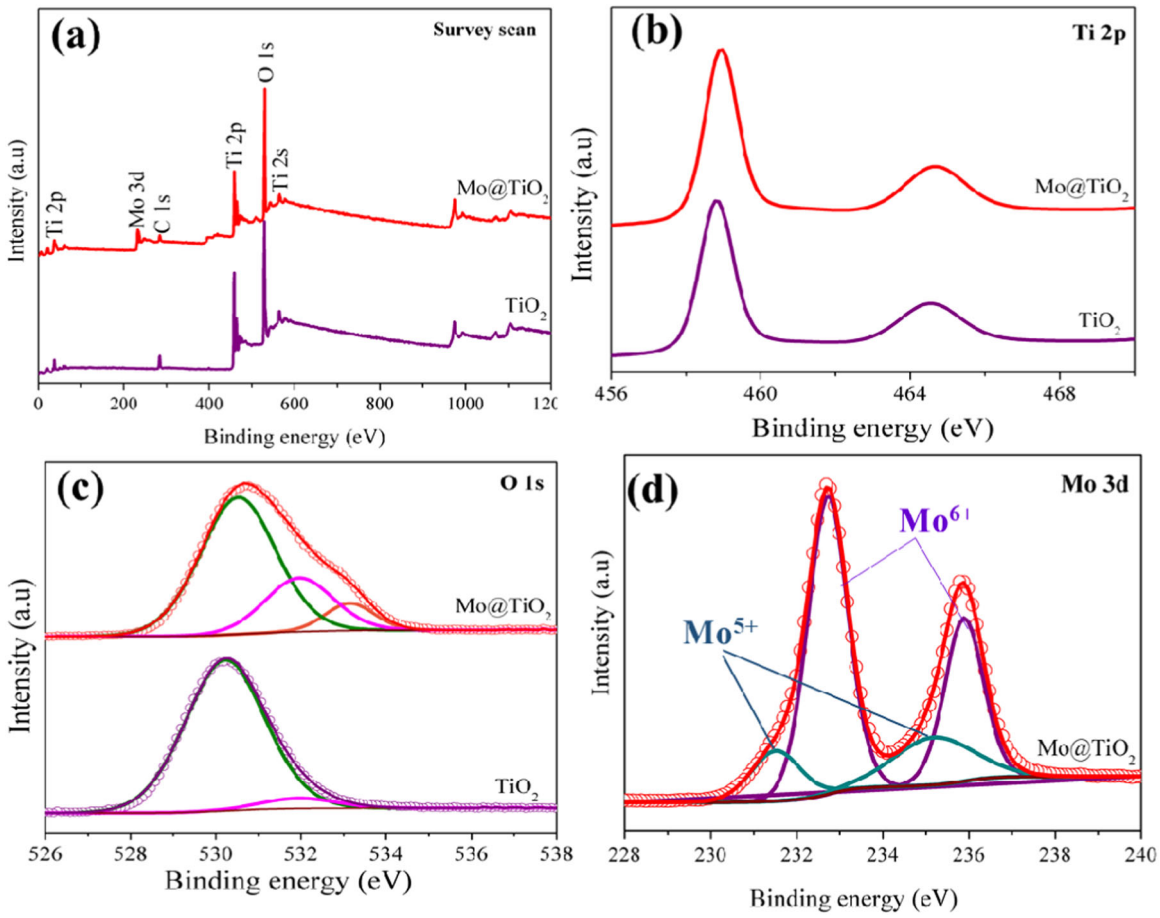

Fig. 3 XPS analyses of the spray pyrolysis-derived TiO_2 and Mo@TiO_2 microspheres. a Survey scan, **b** Ti 2p, **c** O 1 s, **d** Mo 3d

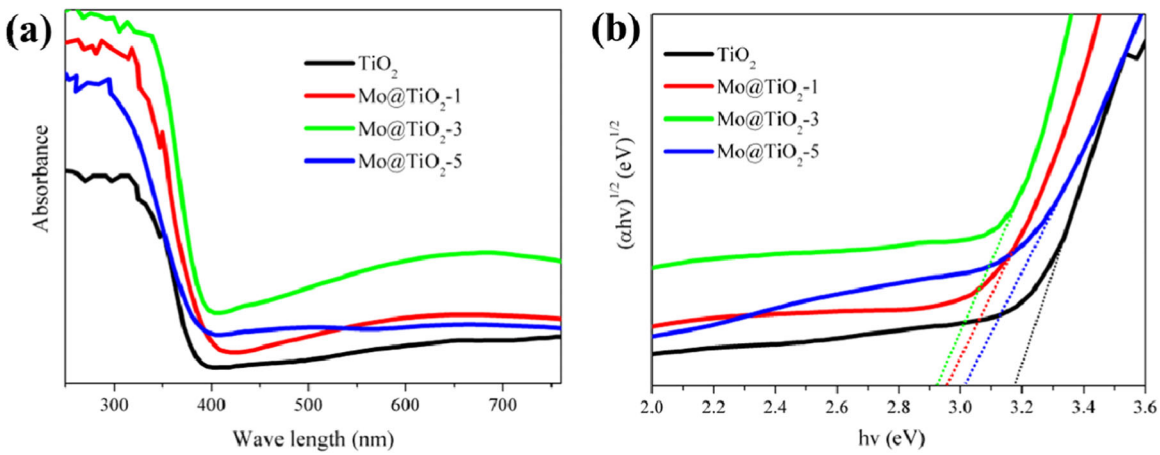

Fig. 4 Optical properties of TiO_2 and Mo@TiO_2 samples. a UV–vis diffuse reflection spectroscopy (DRS) and **b** Tauc's plots

narrowed the bandgap structure because the orbital energy of Mo 4d is quite close to that of Ti 3d [47, 52]. In addition, Mo-doping causes crystal defects inside the host (*e.g.*, oxygen vacancies), which greatly enhance the catalyst's light absorption ability and suppress the recombination of the photo-induced electrons and holes [26, 47]. The findings in the present work revealed that Mo species were finely incorporated into the TiO_2 microspheres under spray pyrolysis conditions. Furthermore, the incorporated Mo dopants enhanced the light absorption ability and created oxygen deficiencies in the fabricated Mo@TiO_2 microspheres, which are favorable for the photo-reduction performance.

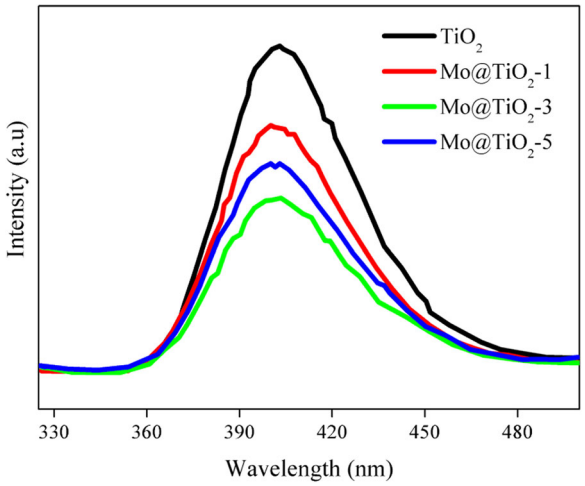

Fig. 5 The photoluminescent spectra of the TiO_2 and Mo@TiO_2 microspheres

The photoluminescence spectra of the prepared Mo@TiO_2 microspheres were analyzed, and the results are depicted in Fig. 5. All catalysts showed a broad peak located around 405 nm, which is caused by the recombination of the photo-generated holes and electrons. As expected, the prepared Mo@TiO_2 catalysts exhibited reduced PL peak intensities compared to the pristine TiO_2. This suggests that the incorporated Mo species suppressed the recombination of photo-generated holes and electrons during light irradiation. These results were consistent with the above findings that Mo-doping disturbed the Ti-O bonds and created the oxygen vacancies in the TiO_2 lattice. These vacancies reportedly aid in trapping and localizing the photo-induced species during light illumination [24, 45].

3.2 Adsorption-photocatalytic degradation of antibiotics

The adsorption-photo-reduction experiments were conducted over the prepared TiO_2, Mo@TiO_2, and P25. Figure 6(a) shows the UV-vis absorption spectrum of tetracycline as a function of sampling time. Figure 6(b) shows the calculated removal efficiency of TE over the commercial TiO_2 and the spray pyrolysis-derived Mo@TiO_2 microspheres. At the pre-adsorption stage, the spray pyrolysis TiO_2 microspheres exhibited considerably greater adsorption ability toward TE than the commercial one. This is possible because the prepared TiO_2 microspheres had higher surface area and pore volume than the commercial titania. Furthermore, spray pyrolysis-derived Mo@TiO_2 exhibited increased adsorption ability toward tetracycline compared to the bare anatase. Specifically, the removal yield of TE by the adsorption over the prepared microspheres TiO_2, Mo@TiO_2-1, Mo@TiO_2-3, and Mo@TiO_2-5 were ~15, 21, 26%, and 29%, respectively [Fig. 6(b)], which were positively correlated with their porosities as mentioned above.

The photodegradation of tetracycline antibiotics was performed under UV light irradiation. As shown in Fig. 6(b), the commercial TiO_2 exhibited a modest TE removal efficiency of *ca.* ~40%, and that value for the undoped TiO_2 microspheres was approximately 62%. As expected, the Mo-incorporated TiO_2 catalysts exhibited improved photo-reduction efficiency than unmodified TiO_2 and exceeded the commercial catalyst. After 160 min UV-light illumination, the total removal efficiency of TE over the prepared Mo@TiO_2-1, Mo@TiO_2-3, and Mo@TiO_2-5 was approximately 67, 90, and 79%, respectively. Such improved photooxidation ability of the Mo@TiO_2 microsphere can be attributable to the synergistic effect of introducing Mo species into the TiO_2 by spray pyrolysis. As discussed above, the prepared Mo@TiO_2 contained surface oxygen vacancies, which increased the light absorption and accelerated the separation of the photo-excited charge carriers. Furthermore, the incorporated Mo species created more pore spaces that facilitated the accumulation of organic pollutants onto the catalyst surface. The obtained results indicated that the photo-reduction efficiency depended on the Mo content introduced into the TiO_2 host, and the catalyst containing 3.0 wt% Mo showed the most excellent photocatalytic efficiency under the investigated conditions. Table 2 compares the TE removal efficiency on various photocatalysts. It can be seen that the spray pyrolysis-derived Mo@TiO_2 catalyst exhibited a comparable removal efficiency compared to some previous samples (see Table 2). Notably, the Mo@TiO_2 microspheres were fabricated by a rapid, facile, and scalable route, thereby making them a promising material for industrial applications.

Reaction kinetic analyses were performed further to reveal the photocatalytic activity of all catalytic samples [Fig. 6(c)]. As presented, the photo-reduction rate of the produced catalysts follows the order: Mo@TiO_2−3 (0.0114 min^{-1}) >Mo@TiO_2-5 (0.00744 min^{-1}) >Mo@TiO_2-1 (0.00638 min^{-1}) >TiO_2 (0.00478 min^{-1}) >P25 (0.00238 min^{-1}). Accordingly, the highest photodegradation rate of ~0.0114 min^{-1} was achieved over the prepared Mo@TiO_2-3 catalyst, which was approximately 2.4 and 4.8 times greater than the pristine TiO_2 microspheres and P25, respectively. Furthermore, the results confirmed that the spray pyrolysis-derived Mo@TiO_2 microspheres effectively degraded the antibiotics under the investigated conditions.

3.3 Effects of experimental conditions

The effects of experimental factors, including catalyst dosage, pollutant concentration, and pH media on the TE removal efficiency, were systematically surveyed. As demonstrated in Fig. 7(a), the photocatalytic yield gradually increased from 55 to 92% with an increase in the catalyst

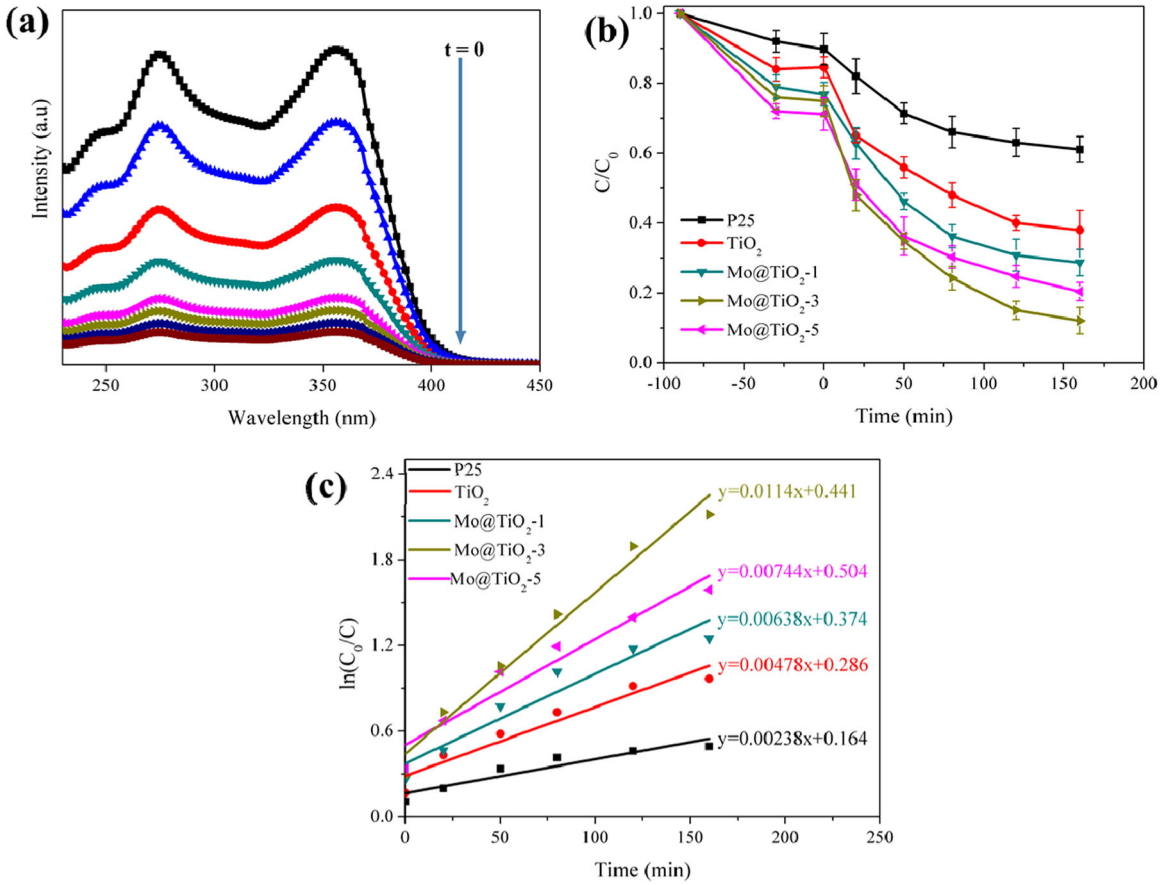

Fig. 6 Adsorption-photocatalytic degradation of TE. a UV-vis absorption of TE, **b** Adsorption-photocatalytic degradation profile of TE, and **c** Pseudo-first-order kinetics of the photo-reduction of TC (Catalyst dosage: 80 mg/L, TE concentration: 60 mg/L, pH = 5)

dosage from 40 to 160 mg L^{-1}, which was attributed to the increasing active sites for adsorption and photooxidation processes. However, further increasing the catalyst dosage to 220 mg L^{-1}, the photocatalytic efficiency diminished to 83%. This phenomenon can be explained by the shielding effect of the light irradiation or self-consumption of the newly formed reactive species by a high catalyst load [46]. In addition, the initial concentration of the antibiotics strongly impacted the photocatalytic performance [Fig. 7(b)]. The prepared Mo@TiO_2 microspheres exhibited optimal photocatalytic performance at the TE concentration of 60 mg L^{-1}. Nonetheless, the removal efficiency diminished by increasing the antibiotic concentration from 120 to 180 mg L^{-1}. This could be because a high concentration of contaminants in the solution could clog the pore spaces of the catalyst. Figure 7(c) depicts the effect of pH media on the removal yield of antibiotics. As revealed, the antibiotics removal efficiency was facilitated in acidic conditions (pH < 6.5) but slowed down in base media (pH > 6.5). The experimental results can be explained via the surface interaction between the catalyst and organic molecules. Indeed, the surface of tetracycline is always negatively charged in the pH range of 2–12; meanwhile, for the synthesized Mo@TiO_2 microspheres, their surfaces were positively charged in acidic media but negatively charged in base media [46]. Here, the surface hydroxyl groups of TiO_2 were involved in the acid-base chemistry of Mo@TiO_2 microspheres, which the following equations:

$$\equiv Ti - OH + H^+ - > - TiOH_2^+$$

$$\equiv Ti - OH + OH^- - > - TiO^- + H_2O$$

Accordingly, low pH media is favorable for the adsorption of antibiotic molecules onto the catalyst surface because of their electrostatic interaction. As a high amount of organic pollutants accumulated on the catalyst, the photoreduction of organic pollutants was facilitated.

3.4 Reusability and stability tests

Stability and reusability are crucial factors that evaluate the prepared materials. Here, the spray-pyrolysis-derived

Table 2 Removal of tetracycline antibiotics over different photocatalysts

Catalyst	Preparation method	Band gap (eV)	Degradation	Light irradiation	Refs.
ZnO/γ-Fe_2O_3	Microwave-assisted hydrothermal	–	~88% degradation after 150 min	UV-visible light	[53]
SnO_2/g-C_3N_4	Hydrothermal	2.45 eV	~92% degradation after 120 min	Visible light	[54]
$MgFe_2O_4$@UiO-66(Zr)	Solvothermal	2.28 eV	~94% degradation after 120 min	Visible light	[2]
TiO_2 -P25	–	–	~91% degradation after 140 min	UV	[55]
N-doped TiO_2	TiO_2-P25 was treated with NH_3 gas at 500 °C for 8 h	–	~87% degradation after 120 min	Visible light	[1]
Mo@TiO_2 microsphere	Spray pyrolysis	2.93 eV	~90% degradation after 160 min	UV	This work

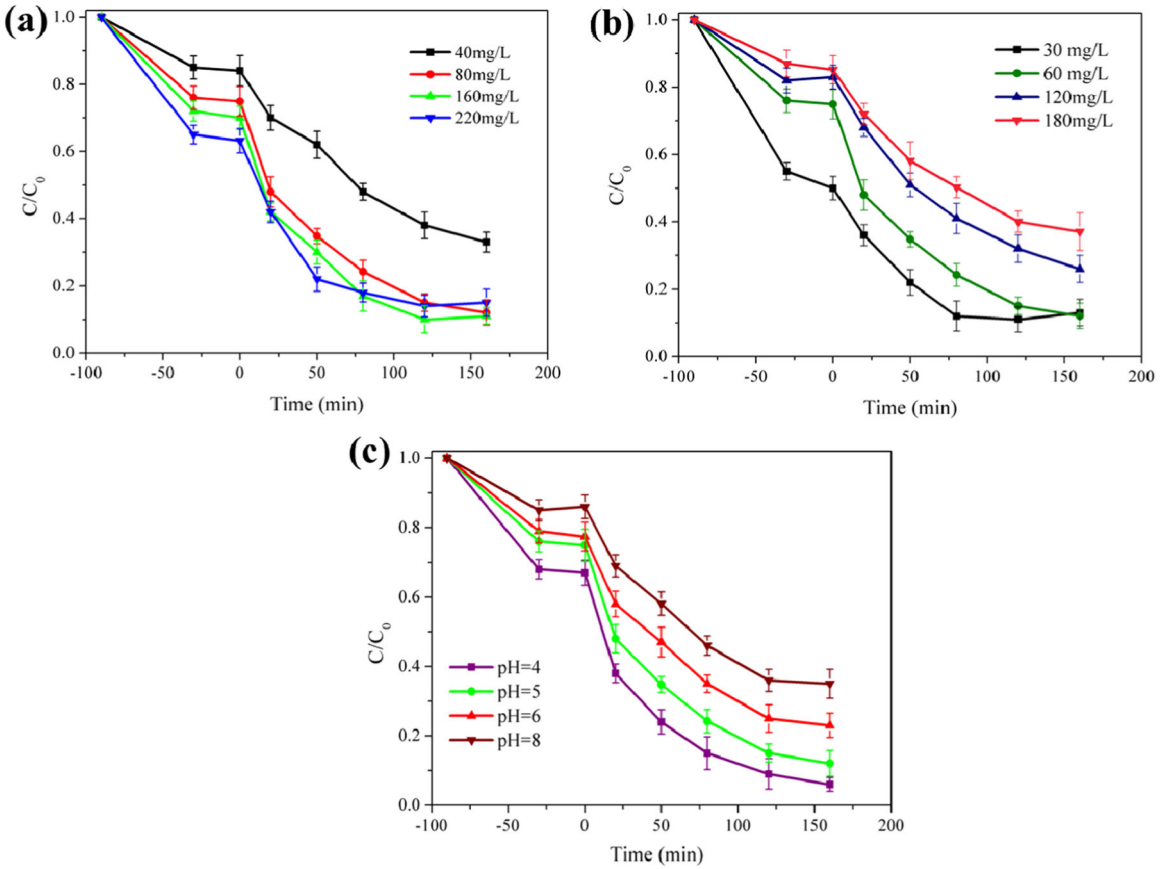

Fig. 7 Effects of experimental factors on the removal of TE over the prepared Mo@TiO_2-3 catalyst. a catalyst dosage, **b** initial concentration of TE, and **c** media pH

Mo@TiO_2 microspheres were reused several times. After use, the Mo@TiO_2-3.0 catalyst was regenerated by washing in deionized water, then drying at 115 °C. As presented in Fig. 8(a), the removal efficiency of TE has unchanged after the first two cycles. After five cycles, the total removal yield reached approximately 78% compared to that of the as-prepared catalyst. This decrease suggests that some intermediate products could strongly bind to the catalyst's active sites, which require higher energy to be desorbed. The morphology and XRD pattern of the used catalyst were examined, and the results are presented in Fig. 8(b) and (c), respectively. Accordingly, the prepared Mo@TiO_2 microspheres maintained their morphology and crystal structure after several cycles. These findings implied that the spray pyrolysis Mo-modified TiO_2 microspheres had good renewability and stability.

4 Conclusions

Mo-modified anatase TiO_2 microspheres were rapidly fabricated by combining sol-gel and spray pyrolysis approaches. Increasing the Mo content onto Mo@TiO_2

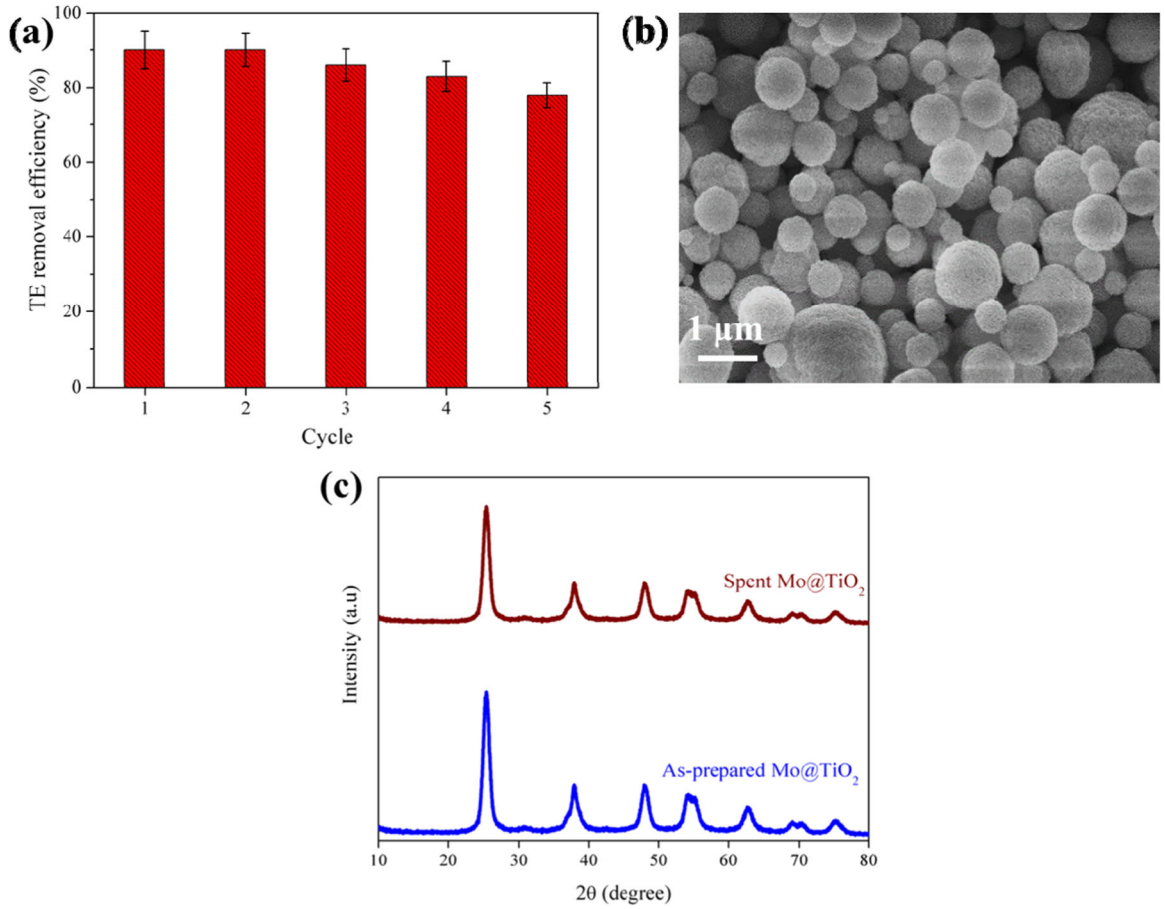

Fig. 8 Regeneration study. a Removal efficiency of tetracycline after five cycles, **b** SEM image of the spent Mo@TiO_2-3 catalyst, and **c** XRD patterns of the Mo@TiO_2-3 catalyst before and after being reused

samples from 1.0 wt% to 5 wt%, the surface area increased from 128 m^2/g to 152 m^2/g, and the pore volume increased from 0.21 cm^3/g to 0.32 cm^3/g, respectively. Under spray pyrolysis conditions, Mo species were effectively incorporated into the lattice of TiO_2, reducing their bandgap energy values. Furthermore, the incorporated Mo dopants created more oxygen deficiencies, which enhanced the photo-reduction ability of the Mo@TiO_2 microspheres compared to the bare TiO_2 and P25. The produced Mo@TiO_2 microspheres loaded 3 wt% of Mo showed the highest tetracycline removal efficiency of *ca.* ~90% after 160 min UV-light illumination. Moreover, the photocatalytic efficiency on the prepared Mo@TiO_2 microspheres was retained after several cyclic experiments. These results indicated that spray pyrolysis-derived Mo@TiO_2 materials could be promising for adsorption-photocatalytic water remediation.

Data availability

The data is true and reliable.

Acknowledgements This research is funded by Vietnam National Foundation for Science and Technology Development (NAFOSTED) under grant number 104.05-2020.32. This work is also supported by the Industrial University of Ho Chi Minh City, Vietnam. The authors are also thankful to Professor Jinsoo Kim at Chemical Engineering Department, Kyung Hee University, Korea, for supporting this work.

Authors contributions The Ky Vo: Conceptualization, investigation, formal analysis, writing manuscript, visualization, editing &r reviewing.

Funding This research is funded by Vietnam National Foundation for Science and Technology Development (NAFOSTED) under grant number 104.05-2020.32

Compliance with ethical standards

Conflict of interest The author declares no competing interests.

Consent to participate All authors agree to participate in the editing of the paper.

Consent to publish All authors agree to publish this manuscript in your journal.

References

1. Wu S, Hu H, Lin Y, Zhang J, Hu YH (2020) Visible light photocatalytic degradation of tetracycline over TiO_2. Chem Eng J 382:122842. https://doi.org/10.1016/j.cej.2019.122842
2. Vo TK, Kim J (2021) Facile synthesis of magnetic framework composite $MgFe_2O_4$@UiO-66(Zr) and its applications in the adsorption–photocatalytic degradation of tetracycline. Environ Sci Pollut Res 28(48):68261–68275. https://doi.org/10.1007/s11356-021-15423-y
3. Zhu X-D, Wang Y-J, Sun R-J, Zhou D-M (2013) Photocatalytic degradation of tetracycline in aqueous solution by nanosized TiO_2. Chemosphere 92(8):925–932. https://doi.org/10.1016/j.chemosphere.2013.02.066
4. Addamo M, Augugliaro V, Paola AD, García-López E, Loddo V, Marcì G, Palmisano L (2005) Removal of drugs in aqueous systems by photoassisted degradation. J Appl Electrochem 35(7):765–774. https://doi.org/10.1007/s10800-005-1630-y
5. Wang Q, Gao Q, Al-Enizi AM, Nafady A, Ma S (2020) Recent advances in MOF-based photocatalysis: environmental remediation under visible light. Inorg Chem Front 7(2):300–339. https://doi.org/10.1039/C9QI01120J
6. The Ky V (2022) Spray pyrolysis synthesis of mesoporous γ-AlOOH and γ-Al_2O_3 microspheres and their properties for Cr (VI) adsorption. Int J Environ Anal Chem:1–21. https://doi.org/10.1080/03067319.2021.2023512
7. Lei X, Li X, Ruan Z, Zhang T, Pan F, Li Q, Xia D, Fu J (2018) Adsorption-photocatalytic degradation of dye pollutant in water by graphite oxide grafted titanate nanotubes. J Mol Liq 266:122–131. https://doi.org/10.1016/j.molliq.2018.06.053
8. Ong CB, Ng LY, Mohammad AW (2018) A review of ZnO nanoparticles as solar photocatalysts: Synthesis, mechanisms and applications. Renew Sust Energ Rev 81:536–551. https://doi.org/10.1016/j.rser.2017.08.020
9. Li G, Lian Z, Wang W, Zhang D, Li H (2016) Nanotube-confinement induced size-controllable g-C_3N_4 quantum dots modified single-crystalline TiO_2 nanotube arrays for stable synergetic photoelectrocatalysis. Nano Energy 19:446–454. https://doi.org/10.1016/j.nanoen.2015.10.011
10. Xu J, Xu J, Jiang S, Cao Y, Xu K, Zhang Q, Wang L (2020) Facile synthesis of a novel Ag3PO4/MIL-100(Fe) Z-scheme photocatalyst for enhancing tetracycline degradation under visible light. Environ Sci Pollut Res 27(30):37839–37851. https://doi.org/10.1007/s11356-020-09903-w
11. Le VN, Vo TK, Yoo KS, Kim J (2021) Enhanced CO_2 adsorption performance on amino-defective UiO-66 with 4-amino benzoic acid as the defective linker. Sep Purif Technol 274:119079. https://doi.org/10.1016/j.seppur.2021.119079
12. Tran NT, Vo TK, Kim J, Othman MR (2021) Esoteric CO adsorption by CuCl-$NiCl_2$ embedded microporous MIL-101 (Cr). Colloids Surf A Physicochem Eng 615:126242. https://doi.org/10.1016/j.colsurfa.2021.126242
13. Vo TK, Kim J-H, Kwon HT, Kim J (2019) Cost-effective and eco-friendly synthesis of MIL-101(Cr) from waste hexavalent chromium and its application for carbon monoxide separation. J Ind Eng Chem 80:345–351. https://doi.org/10.1016/j.jiec.2019.08.013
14. Mirzaeifard Z, Shariatinia Z, Jourshabani M, Rezaei Darvishi SM (2020) ZnO photocatalyst revisited: effective photocatalytic degradation of emerging contaminants using S-Doped ZnO nanoparticles under visible light radiation. Ind Eng Chem Res 59(36):15894–15911. https://doi.org/10.1021/acs.iecr.0c03192
15. Meng J, Chen Q, Lu J, Liu H (2019) Z-Scheme photocatalytic CO_2 reduction on a heterostructure of oxygen-defective ZnO/reduced graphene oxide/UiO-66-NH2 under visible light. ACS Appl Mater Interfaces 11(1):550–562. https://doi.org/10.1021/acsami.8b14282
16. Akhavan O, Mehrabian M, Mirabbaszadeh K, Azimirad R (2009) Hydrothermal synthesis of ZnO nanorod arrays for photocatalytic inactivation of bacteria. J Phys D: Appl Phys 42(22):225305. https://doi.org/10.1088/0022-3727/42/22/225305
17. Koiki BA, Arotiba OA (2020) Cu_2O as an emerging semiconductor in photocatalytic and photoelectrocatalytic treatment of water contaminated with organic substances: a review. RSC Adv 10(60):36514–36525. https://doi.org/10.1039/D0RA06858F
18. Mishra P, Patnaik S, Parida K (2019) An overview of recent progress on noble metal modified magnetic Fe_3O_4 for photocatalytic pollutant degradation and H_2 evolution. Catal Sci Technol 9(4):916–941. https://doi.org/10.1039/C8CY02462F
19. Jana TK, Pal A, Mandal AK, Sarwar S, Chakrabarti P, Chatterjee K (2017) Photocatalytic and antibacterial performance of α-Fe_2O_3 Nanostructures. ChemistrySelect 2(10):3068–3077. https://doi.org/10.1002/slct.201700294
20. Ohko Y, Ando I, Niwa C, Tatsuma T, Yamamura T, Nakashima T, Kubota Y, Fujishima A (2001) Degradation of Bisphenol A in water by TiO_2 photocatalyst. Environ Sci Technol 35(11):2365–2368. https://doi.org/10.1021/es001757t
21. Li J, Zhang M, Guan Z, Li Q, He C, Yang J (2017) Synergistic effect of surface and bulk single-electron-trapped oxygen vacancy of TiO_2 in the photocatalytic reduction of CO_2. Appl Catal B 206:300–307. https://doi.org/10.1016/j.apcatb.2017.01.025
22. Akhavan O, Ghaderi E, Rahimi K (2012) Adverse effects of graphene incorporated in TiO_2 photocatalyst on minuscule animals under solar light irradiation. J Mater Chem 22(43):23260–23266. https://doi.org/10.1039/C2JM35228A
23. Thi TV, Rai AK, Gim J, Kim S, Kim J (2014) Effect of Mo6+ doping on electrochemical performance of anatase TiO_2 as a high performance anode material for secondary lithium-ion batteries. J Alloy Compd 598:16–22. https://doi.org/10.1016/j.jallcom.2014.02.019
24. Dong J, Hu C, Qi W, An X, Liu H, Qu J (2020) Defect-enhanced photocatalytic removal of dimethylarsinic acid over mixed-phase mesoporous TiO_2. Res J Environ Sci 91:35–42. https://doi.org/10.1016/j.jes.2019.12.013
25. Xia T, Zhang W, Wang Z, Zhang Y, Song X, Murowchick J, Battaglia V, Liu G, Chen X (2014) Amorphous carbon-coated TiO_2 nanocrystals for improved lithium-ion battery and photocatalytic performance. Nano Energy 6:109–118. https://doi.org/10.1016/j.nanoen.2014.03.012
26. Erdogan N, Park J, Ozturk A (2016) Synthesis and enhanced photocatalytic activity of molybdenum, iron, and nitrogen triple-doped titania nanopowders. Ceram Int 42(15):16766–16774. https://doi.org/10.1016/j.ceramint.2016.07.158
27. Shayegan Z, Lee C-S, Haghighat F (2018) TiO_2 photocatalyst for removal of volatile organic compounds in gas phase – A review. Chem Eng J 334:2408–2439. https://doi.org/10.1016/j.cej.2017.09.153
28. Akhavan O (2009) Lasting antibacterial activities of Ag–TiO_2/Ag/a-TiO_2 nanocomposite thin film photocatalysts under solar light irradiation. J Colloid Interface Sci 336(1):117–124. https://doi.org/10.1016/j.jcis.2009.03.018
29. Akhavan O (2010) Thickness dependent activity of nanostructured TiO_2/α-Fe_2O_3 photocatalyst thin films. Appl Surf Sci 257(5):1724–1728. https://doi.org/10.1016/j.apsusc.2010.09.005
30. Akhavan O, Ghaderi E (2009) Photocatalytic reduction of graphene oxide nanosheets on TiO_2 thin film for photoinactivation of bacteria in solar light irradiation. J Phys Chem C 113(47):20214–20220. https://doi.org/10.1021/jp906325q

31. Yu X, Fan X, An L, Liu G, Li Z, Liu J, Hu P (2018) Meso-crystalline Ti_3+TiO_2 hybridized g-C_3N_4 for efficient visible-light photocatalysis. Carbon 128:21–30. https://doi.org/10.1016/j.carbon.2017.11.078
32. Ganguly P, Mathew S, Clarizia L, Kumar RS, Akande A, Hinder SJ, Breen A, Pillai SC (2020) Ternary metal chalcogenide heterostructure ($AgInS_2$–TiO_2) nanocomposites for visible light photocatalytic applications. ACS Omega 5(1):406–421. https://doi.org/10.1021/acsomega.9b02907
33. Akhavan O, Abdolahad M, Abdi Y, Mohajerzadeh S (2009) Synthesis of titania/carbon nanotube heterojunction arrays for photoinactivation of E. coli in visible light irradiation. Carbon 47(14):3280–3287. https://doi.org/10.1016/j.carbon.2009.07.046
34. Phromma S, Wutikhun T, Kasamechonchung P, Eksangsri T, Sapcharoenkun C (2020) Effect of calcination temperature on photocatalytic activity of synthesized TiO_2 nanoparticles via wet ball milling sol-gel method. Appl Sci 10(3):993
35. Devi LG, Murthy BN, Kumar SG (2009) Photocatalytic activity of V5+, Mo6+ and Th4+ doped polycrystalline TiO_2 for the degradation of chlorpyrifos under UV/solar light. J Mol Catal A Chem 308(1):174–181. https://doi.org/10.1016/j.molcata.2009.04.007
36. Štengl V, Bakardjieva S (2010) Molybdenum-doped anatase and its extraordinary photocatalytic activity in the degradation of Orange II in the UV and vis regions. J Phys Chem C 114(45):19308–19317. https://doi.org/10.1021/jp104271q
37. Vo TK, Kim W-S, Kim S-S, Yoo KS, Kim J (2018) Facile synthesis of Mo/Al_2O_3–TiO_2 catalysts using spray pyrolysis and their catalytic activity for hydrodeoxygenation. Energy Convers Manag 158:92–102. https://doi.org/10.1016/j.enconman.2017.12.049
38. Vo TK, Le VN, Quang DT, Kim J (2021) Facile synthesis of spray pyrolysis-derived CuCl/γ-Al_2O_3 microspheres and their properties for CO adsorption and CO/CO_2 separation. Microporous Mesoporous Mater 321:111132. https://doi.org/10.1016/j.micromeso.2021.111132
39. Ji J, Im K, An H, Yoo SJ, Chung Y, Kim J, Kwon Y (2022) Spray pyrolysis-assisted synthesis of hollow cobalt nitrogen-doped carbon catalyst for the performance enhancement of membraneless fuel cells. Int J Energy Res 46(2):760–773. https://doi.org/10.1002/er.7200
40. Han S, Yoo KS, Kim D, Kim J, Othman MR (2021) Metal-silica spherical particles development by spray pyrolysis: Effect of metal species on surface area and toluene adsorption. J Anal Appl Pyrolysis 156:105049. https://doi.org/10.1016/j.jaap.2021.105049
41. Phan D-P, Vo TK, Le VN, Kim J, Lee EY (2020) Spray pyrolysis synthesis of bimetallic NiMo/Al_2O_3–TiO_2 catalyst for hydrodeoxygenation of guaiacol: Effects of bimetallic composition and reduction temperature. J Ind Eng Chem 83:351–358. https://doi.org/10.1016/j.jiec.2019.12.008
42. Zhang J, Xi J, Ji Z (2012) Mo+N Codoped TiO_2 sheets with dominant {001} facets for enhancing visible-light photocatalytic activity. J Mater Chem 22(34):17700–17708. https://doi.org/10.1039/C2JM32391E
43. Majeed J, Nayak C, Jha SN, Bhattacharyya K, Bhattacharyya D, Tripathi AK (2015) Correlation of Mo dopant and photocatalytic properties of Mo incorporated TiO_2: an EXAFS and photocatalytic study. RSC Adv 5(110):90932–90940. https://doi.org/10.1039/C5RA14613E
44. Ly HV, Im K, Go Y, Galiwango E, Kim S-S, Kim J, Choi JH, Woo HC (2016) Spray pyrolysis synthesis of γ-Al_2O_3 supported metal and metal phosphide catalysts and their activity in the hydrodeoxygenation of a bio-oil model compound. Energy Convers Manag 127:545–553. https://doi.org/10.1016/j.enconman.2016.09.020
45. Li J, Zhou H, Zhuo H, Wei Z, Zhuang G, Zhong X, Deng S, Li X, Wang J (2018) Oxygen vacancies on TiO_2 promoted the activity and stability of supported Pd nanoparticles for the oxygen reduction reaction. J Mater Chem A 6(5):2264–2272. https://doi.org/10.1039/C7TA09831F
46. Vo TK, (2022) Spray pyrolysis synthesis and UV-driven photocatalytic activity of mesoporous Al_2O_3@TiO_2 microspheres. Environ Sci Pollut Res. https://doi.org/10.1007/s11356-022-18865-0
47. Wang S, Bai LN, Sun HM, Jiang Q, Lian JS (2013) Structure and photocatalytic property of Mo-doped TiO_2 nanoparticles. Powder Technol 244:9–15. https://doi.org/10.1016/j.powtec.2013.03.054
48. Deng H, Wang Y, Zhang X, Kou X, Chen B, Zhu C (2019) Photodegradation under natural indoor weak light assisted adsorption of X-3B on TiO_2/Al2O_3 nanocomposite. Chem Eng J 372:99–106. https://doi.org/10.1016/j.cej.2019.04.079
49. Kondekar NP, Boebinger MG, Woods EV, McDowell MT (2017) In Situ XPS investigation of transformations at crystallographically oriented MoS_2 interfaces. ACS Appl Mater Interfaces 9(37):32394–32404. https://doi.org/10.1021/acsami.7b10230
50. Saadati M, Akhavan O, Fazli H (2021) Single-layer MoS_2-MoO_{3-x} heterojunction nanosheets with simultaneous photoluminescence and co-photocatalytic features. Catalysts 11(12):1445
51. Zhang Y, Yu X, Liu H, Lian X, Shang B, Zhan Y, Fan T, Chen Z, Yi X (2021) Controllable synthesis of the defect-enriched MoO_{3-x} nanosheets as an effective visible-light photocatalyst for the degradation of organic dyes. Environ Sci Nano 8(7):2049–2058. https://doi.org/10.1039/D1EN00210D
52. Gai Y, Li J, Li S-S, Xia J-B, Wei S-H(2009) Design of narrow-gap TiO_2: a passivated codoping approach for enhanced photoelectrochemical activity Phys Rev Lett 102(3):036402. https://doi.org/10.1103/PhysRevLett.102.036402
53. Semeraro P, Bettini S, Sawalha S, Pal S, Licciulli A, Marzo F, Lovergine N, Valli L, Giancane G (2020) Photocatalytic degradation of tetracycline by ZnO/γ-$Fe_{(2)}O_{(3)}$ paramagnetic nanocomposite material. Nanomaterials 10(8):1458. https://doi.org/10.3390/nano10081458
54. Oluwole AO, Olatunji OS (2022) Photocatalytic degradation of tetracycline in aqueous systems under visible light irridiation using needle-like SnO2 nanoparticles anchored on exfoliated g-C3N4. Environ Sci Eur 34(1):5. https://doi.org/10.1186/s12302-021-00588-7
55. Safari GH, Hoseini M, Seyedsalehi M, Kamani H, Jaafari J, Mahvi AH (2015) Photocatalytic degradation of tetracycline using nanosized titanium dioxide in aqueous solution. Int J Environ Sci Technol 12(2):603–616. https://doi.org/10.1007/s13762-014-0706-9